Available online at www.sciencedirect.com
ScienceDirect
Journal of Power Sources 169 (2007) 47–52
JOURNAL OF POWER SOURCES
www.elsevier.com/locate/jpowsour

Short communication

Preparation and characterisation of SOFC anodic materials based on Ce–Cu☆

A. Fuerte[a,*], R.X. Valenzuela[a], L. Daza[a,b]

[a] *CIEMAT, Departamento de Energía, Av. Complutense 22, 28040 Madrid, Spain*
[b] *Instituto de Catálisis y Petroleoquímica (CSIC), Marie Curie 2, Campus Cantoblanco, 28049 Madrid, Spain*

Available online 19 March 2007

Abstract

Ce–Cu mixed oxide precursors with varing Ce:Cu atomic ratio have been prepared by freeze-drying and microemulsion coprecipitation methods. Nanostructured particles having different properties have been obtained. Physicochemical properties have been studied with X-ray diffraction, UV–vis spectroscopy, nitrogen adsorption–desorption, mercury intrusion porosimetry, ICP-AES, conductivity measurement and thermal expansion coefficient. All samples show fluorite structure with slight copper surface enrichment for samples having high copper content. Microemulsion method allows the introduction of a large quantity of copper into the cerium oxide structure, obtaining a nanostructured mixed oxide of high surface area. On the other hand, freeze-drying samples does not show evidence of copper incorporation to the lattice of cerium oxide. All materials have a thermal expansion coefficient similar to other components of SOFC.

Keywords: SOFC anodes; Ce–Cu mixed oxides; Freeze-drying; Microemulsion coprecipitation

1. Introduction

Nickel–zirconia cermet is the most common anode for solid oxide fuel cells (SOFC), due to goal electrochemical behaviour and high catalytic activity. However, this material shows some drawbacks, the most important of which is the carbon deposition on the anode surface catalysed by nickel when hydrocarbon fuels are used, instead of pure hydrogen. The formation of these carbon deposits could be avoided by replacing nickel for other electrical conductor. In this sense, copper–ceria-based anodes have recently received a special interest [1]. Copper is a relative inert metal for carbon deposition reactions and provides electrical conductivity to the anode. On the other hand, it is necessary to add an active phase, ceria, to the anode in order to achieve reasonable performance [2]. Examples of this type of composite anode have shown effective behaviour with a variety of hydrocarbon fuels [3], and are highly resistant to deactivation by carbon deposition, even considering the direct conversion of hydrocarbon fuels without previous reforming to CO and H_2 [4]. These Cu-based anodes have the additional advantage of being reasonably tolerant to sulphur [5].

Preparation of Ce–Cu-based anodes has required the development of new synthetic methods, different from those used to produce Ni–YSZ cermet, in order to control the microstructure, which is a principal characteristic determining electrode activity.

A series of Ce–Cu-based materials has been synthesised by two methods, freeze-drying and microemulsion coprecipitation. Both methods allow for the control of structure of materials to a certain degree. We studied the influence of the synthesis method employed on the physicochemical characteristics of the materials and the influence of the doping level of copper on their structure. The effect caused by the incorporation of ion Cu^{2+} to the lattice of cerium oxide on the structure and properties is explored in this report and focused on the use of these new materials as SOFC anodes capable to work using alternative fuels. It will be shown that preparation method based on microemulsion coprecipitation allows insertion of up to ca. 21 at.% Cu in substitutional positions of the fluorite structure. To assist in interpreting the main characterisation of new materials, reference systems consisting of CeO_2, which were prepared following the same two synthetic methods, were also analysed.

☆ This paper presented at the 2nd National Congress on Fuel Cells, CONAPPICE 2006, Madrid, Spain, 18–20 October 2006.

* Corresponding author. Fax: +34 91 346 6269.
E-mail address: araceli.fuerte@ciemat.es (A. Fuerte).

0378-7753/$ – see front matter © 2007 Elsevier B.V. All rights reserved.
doi:10.1016/j.jpowsour.2007.03.033

2. Experimental

2.1. Synthesis of materials

Cu–CeO_2 binary oxides samples, having copper content between 5 and 25 at.%, were prepared by freeze-drying [6] and microemulsion coprecipitation methods [7]. Following the preparation method, the amorphous Ce–Cu material was calcined under air for 2 h at 723 K. Samples are hereafter named ACu*x*, *x* being the Cu atomic content and A specifying the preparation method (F for freeze-drying and M for microemulsion coprecipitation). CeO_2 was prepared following both methods as reference material.

For freeze-drying prepared samples, FCu*x*, initial standardised nitrate acetic acid solutions were mixed in the corresponding ratio. Droplets of this solution were flash frozen by projection on liquid nitrogen and then freeze-dried at a pressure of 1–10 Pa in a Telstar Cryodos freeze-drier.

MCu*x* samples were prepared by precipitation within a reverse microemulsion. For this, a microemulsion containing *n*-heptane as organic solvent, Triton X-100 (Aldrich) as surfactant, hexanol as cosurfactant and an aqueous solution of appropriate amounts of the cerium and copper nitrates, were mixed with another similar microemulsion in which the aqueous component was a tetramethylammonium hydroxide solution as precipitant agent. Upon mixing, oxides precipitated inside the aqueous droplets. After stirring, solid was isolated by centrifugation, rinsed and dried at 383 K for 24 h and finally calcined in air at 773 K.

2.2. Physicochemical characterisation of materials

2.2.1. Chemical and textural characterisation

Ce:Cu composition was analysed via inductively coupled plasma-atomic emission spectroscopy (ICP-AES), after selective chemical attack of samples by various media, such as NaOH and concentrated acids. The specific surface area measurements were obtained by nitrogen absorption isotherm, at 77 K, using a Micrometrics ASAP 2010 equipment. Porosity and pore size distribution were determined by Mercury intrusion porosimetry, with a Micrometrics Pore Sizer 9310.

2.2.2. X-ray powder diffraction (XRD)

XRD patterns were recorded at room temperature using an step scan procedure (0.05°/2θ step, time per step 0.5 or 1 s) in the 2θ range 20–100° on a Seifert diffractometer equipped with a crystal monochromator employing Cu Kα radiation (λ = 1.5418 Å). The crystallite size (D_β) of materials was determined from line-broadening measurements on the (1 1 1) peak of CeO_2, using the Scherrer equation,

$$D_\beta = \frac{K\lambda}{\beta \cos\theta} \quad (1)$$

2.2.3. UV–vis spectroscopy

UV–vis diffuse reflectance spectroscopy experiments were performed with a Shimadzu UV-2401 spectrometer, in the wavelength range of 200–800 nm. $BaSO_4$ was used as a blank material. The percentage of reflectance was converted into $f(R)$ values using a Kubelka–Munk transform. The spectra were collected at room temperature, using sample ground into powder with no other pre-treatment.

2.2.4. Thermal expansion measurements

Thermal expansion coefficients (TEC) were measured on an alumina dilatometer Linseis L75/1550, from room temperature to 973 K, with a heating rate of 5 K min^{-1} and a 2 h dwell time at maximum temperature. Previous to these measurements, samples were calcined for 2 h to 1023 K and cold pressed into pellets (10 mm in diameter and 0.9 mm thickness) at 2 tonnes cm^{-2}.

2.2.5. Conductivity measurements

Electrical conductivity was measured using electrochemical impedance spectroscopy, by the two-probe method with an Autolab Galvanostat/Potentiostat PGSTAT30 equipment with a frequency response analyser. Frequencies were varied from 1 to 10 MHz with 5 mV amplitude. Measurements were carried out from 573 to 1023 K in air. For this purpose as-prepared samples were cold pressed into pellets, following similar method detailed above for thermal expansion measurements. The sintered pellets were coated with gold paste (TR 1531) on the pellet surfaces in order to facilitate good electrical contact. The conductivity was calculated using the formula:

$$\sigma = \frac{1e}{RS} \quad (2)$$

where S is the electrode area, e the separation distance between electrodes (usually the sample thickness) and R is the resistance in the sample and it was directly given by the intersection of semi-circle with the real axis for each temperature in the Nyquist representation.

3. Results and discussion

Two synthetic methods, freeze-drying and microemulsion coprecipitation, have been used to obtain Ce–Cu binary oxides. The main characterisation results are detailed in Table 1. Copper content in new materials is close to nominal value, except in the case of MCu25 where only 21 at.% Cu was detected. X-ray diffraction (Figs. 1 and 2) gives evidence that all samples contain ceria in mainly fluorite-type structure with crystallinity generally decreasing with the copper content. Average crystallite size of CeO_2 (reference materials) and Ce–Cu binary oxides, calculated from the Scherrer method, varies from 4 to 10 nm, being slightly smaller for MCu*x* samples. The presence of diffraction peaks at 35.7° and 38.9° in diffractograms for high copper content samples (>20%) provides evidence of the formation of an additional phase, attributed to monoclinic CuO. No peaks corresponding to either copper metal or copper oxides are detected. XRD profiles show that the presence of copper induces a decrease in the lattice parameter (a) for MCu*x* samples, in Table 1 lattice parameter values have been listed along with those of CeO_2. No variation was observed in the case of FCu*x* materials, the lattice parameter was kept constant with increasing copper content. Considering

Table 1
Main characterisation results of Ce–Cu mixed oxides and reference materials

Sample	Copper content[a] (Cu at.%)	BET surface area ($m^2\ g^{-1}$)	Crystal size[b] (nm)	Lattice parameter[b], a (Å)
$FCeO_2$	0	114.9	9.5	5.4098
FCu5	5	72.8	8.4	5.4098
FCu10	10	113.7	7.9	5.4098
FCu15	11	106.7	6.2	5.4098
FCu20	20	104.6	6.5	5.4098
FCu25	25	82.8	5.5	5.4098
$MCeO_2$	0	107.9	5.9	5.4162
MCu5	5	157.6	5.7	5.3966
MCu10	10	160.7	5.1	5.3963
MCu15	16	190.7	4.2	5.3828
MCu20	21	135.7	4.5	5.3828
MCu25	21	190.8	3.7	5.3757

[a] Cation basis [100 × Cu/(Cu + Ce)] by ICP-AES.
[b] Measured by XRD, for fluorite-type structure.

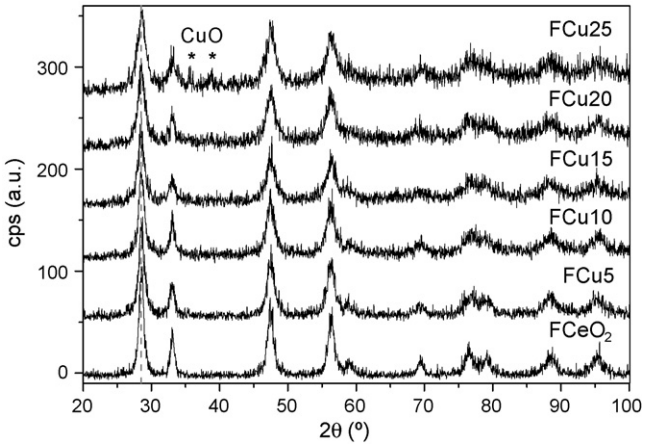

Fig. 1. XRD spectra of FCux samples and $FCeO_2$ reference; *CuO peaks.

the ionic radius of Cu^{2+} (0.73 Å) and that of Ce^{4+} (0.97 Å), a large decrease in the lattice parameter should be expected with the increase in Cu^{2+} ions substitution in the fluorite lattice. But, simultaneously an increase in the oxygen vacancy is promoted

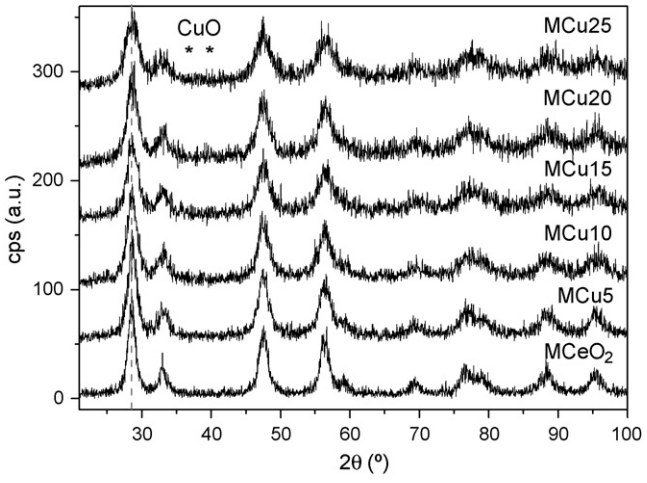

Fig. 2. XRD spectra of MCux samples and $MCeO_2$ reference; *CuO peaks.

for the substitution of Ce^{4+} with Cu^{2+} ions, therefore, only a small decrease in lattice parameter a is observed. This fact indicates that up to 21 at.% of Cu^{2+} can be introduced in CeO_2, forming a solid solution of $Ce_{1-x}Cu_xO_{2-\delta}$, in the case of samples prepared by microemulsion method (MCux). Higher copper content (>21%) entails the formation of CuO that remains on ceria surface.

Both methods are useful for obtaining Ce–Cu samples, after 723 K calcination, with surface areas ca. 110–190 $m^2\ g^{-1}$, see Table 1. These values are much higher than published analogues [8]. For MCux binary oxides, an increase in surface area, or decrease in crystallite size, is observed with the increase of the Cu/(Ce + Cu) ratio, however, no significant changes are produced in surface area of FCux samples. The dependence of the pore volume on the copper content is consistent with that of the BET area. The N_2 adsorption–desorption experiments show an uniform pore size distribution, in the range from 4 to 8 nm, for materials prepared by microemulsion method, MCux, whereas freeze-drying prepared samples, FCux, have a similar pore size but their distribution is not homogeneous.

The presence of copper also has influence on the electronic properties of the synthesised materials. UV–vis spectra of the Ce–Cu samples and CeO_2 reference materials are shown in Figs. 3 and 4. Two broad bands at 270 and 354 nm, respectively, are observed for CeO_2 and FCux samples, no contribution from CuO can be detected. In the case of MCux materials, the constant band at 270 nm can be ascribed to the intrinsic character of CeO_2, while the adsorption edge at 367 nm is blue-shifted and weakened. This blue shift may indicate the formation of CeO_2–CuO solid solution, which results in the increasing of splitting between appropriate electron levels and, as a consequence, increasing energy of transition. So, it can be concluded that the 367 nm band is related to defects in the cerium oxide structure. The shift and the intensity reduction of the 367 nm band might be ascribed to the enhanced defect structure due to the formation of $Ce_{1-x}Cu_xO_{2-\delta}$ solid solutions [9].

One characteristic that determines the validity or not for using a material in high temperature fuel cells (SOFCs and IT-SOFCs) is the thermal expansion coefficient (TEC), which in turn must

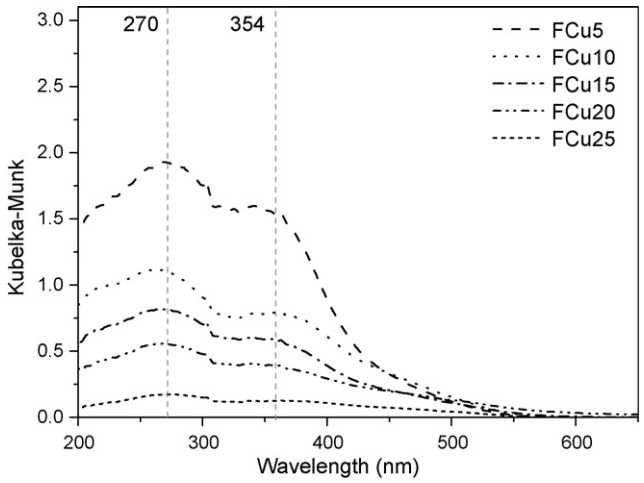

Fig. 3. UV–vis spectra of FCu*x* samples.

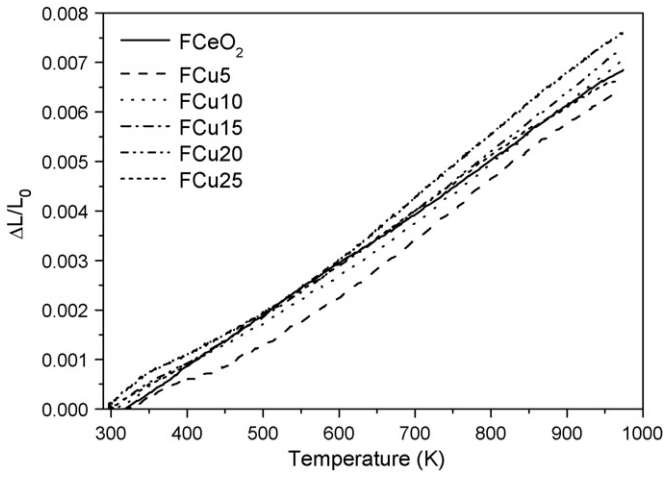

Fig. 5. Thermal expansion behaviour of FCu*x* samples and $FCeO_2$ references in the temperature range of 293–923 K.

Table 2
Thermal expansion coefficients of Ce–Cu mixed oxides and reference materials

Sample	TEC (K^{-1})	Sample	TEC (K^{-1})
$FCeO_2$	10.55×10^{-6}	$MCeO_2$	10.09×10^{-6}
FCu5	11.30×10^{-6}	MCu5	12.81×10^{-6}
FCu10	11.28×10^{-6}	MCu10	12.94×10^{-6}
FCu15	12.30×10^{-6}	MCu15	12.50×10^{-6}
FCu20	11.50×10^{-6}	MCu20	11.83×10^{-6}
FCu25	10.51×10^{-6}	MCu25	13.02×10^{-6}

be similar to the electrolyte, in order to prevent the degradation of these cells in the heating and cooling processes. The results of thermal expansion for FCu*x* and MCu*x* series, respectively, are presented in Figs. 5 and 6, being reported as relative thermal expansion versus temperature. The values of thermal expansion coefficients for FCu*x* and MCu*x* series and CeO_2 reference materials were estimated from the slope of a linear region from 473 K, and they are listed in Table 2. TEC values vary from 10×10^{-6} to $13 \times 10^{-6}\,K^{-1}$, having minimum differences in relation with copper content. It should be noted that Cu-doped samples showed a slight higher value than reference materials ($FCeO_2$ and $MCeO_2$). The linear thermal expansion coefficients for Cu-doped ceria, FCu*x* and MCu*x*, are closely matched to the common SOFC and IT-SOFC electrolyte material ($11 \times 10^{-6}\,K^{-1}$ for 8YSZ [10] and $11.9 \times 10^{-6}\,K^{-1}$ for CGO [11], respectively). Thus, new synthesised materials are in the thermal compatibility range with usual components of SOFC.

Although, electrical behaviour of these materials should be analysed under real conditions of operation for SOFC anodes, and it will be realised in short-term, a preliminary study of that has been tackled under air atmosphere. The apparent conductivity of compacted samples was found to increase with temperature, see Figs. 7 and 8. These values are in good agreement with those found in literature [12]. In general, MCu*x* samples show higher values for electrical conductivity than FCu*x* samples. It should be noted that a substantial increase is observed in values of electrical conductivity with an increasing copper content (Fig. 9). This effect is much more significant in those samples, where Cu^{2+} has successfully substituted cerium

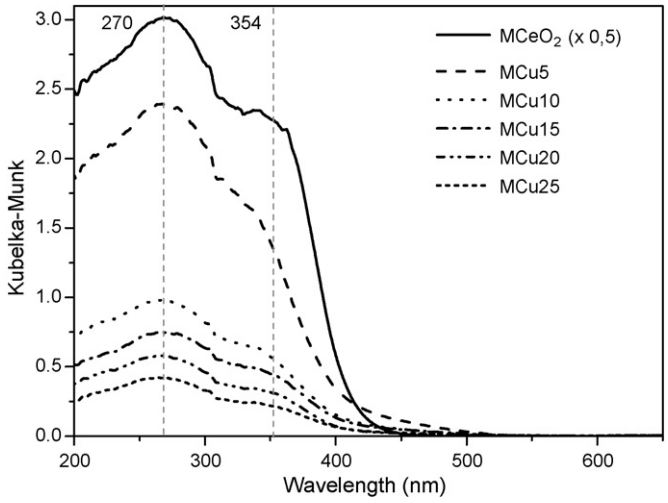

Fig. 4. UV–vis spectra of MCu*x* samples and $MCeO_2$ reference.

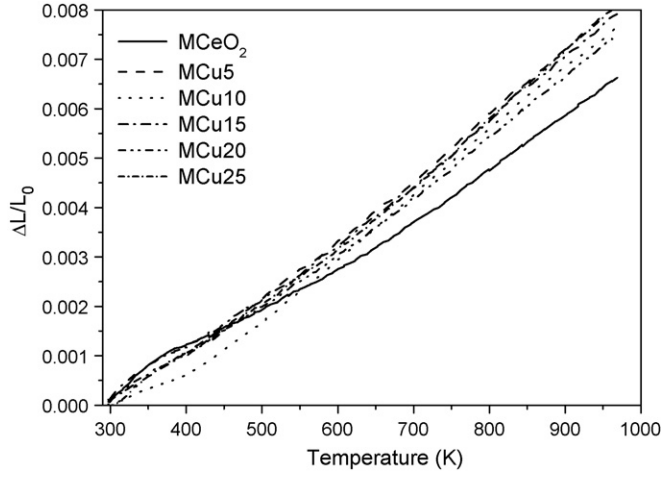

Fig. 6. Thermal expansion behaviour of MCu*x* samples and $MCeO_2$ references in the temperature range of 293–923 K.

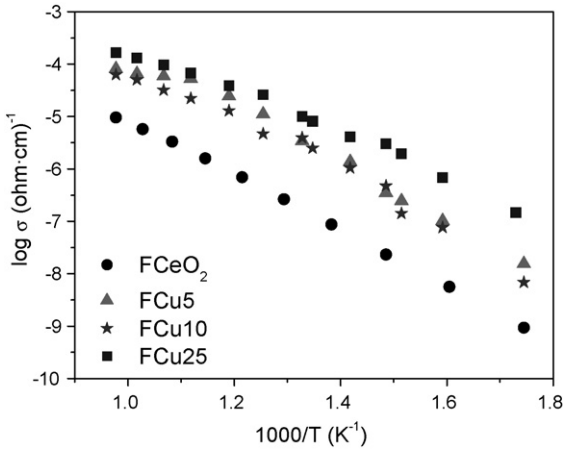

Fig. 7. log σ vs. 1000/T plots for FCux oxides and $FCeO_2$ references in the temperature range of 573–1023 K in air.

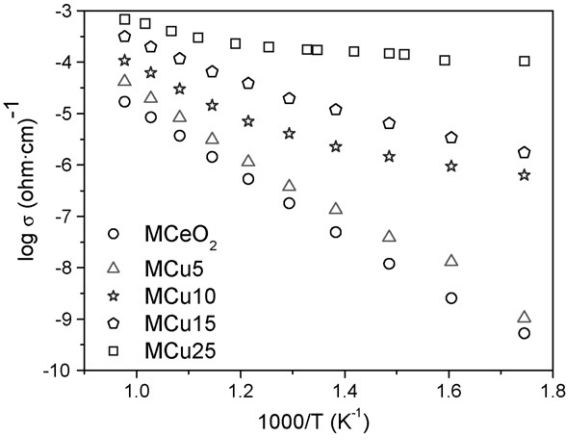

Fig. 8. log σ vs. 1000/T plots for MCux and $MCeO_2$ references in the temperature range of 573–1023 K in air.

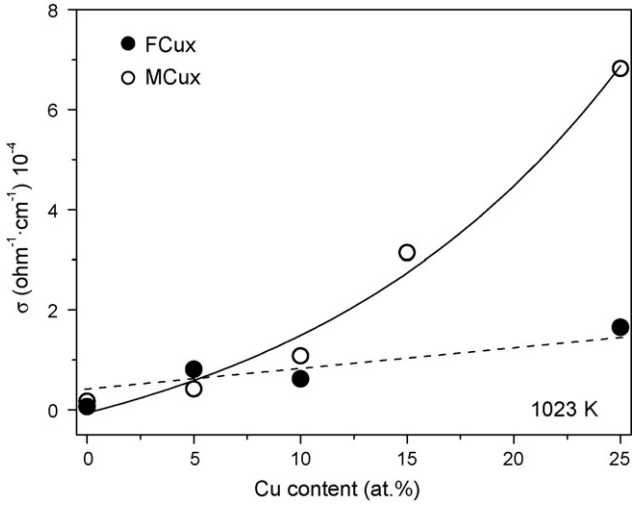

Fig. 9. Dependence of electrical conductivity on copper content of Ce–Cu mixed oxides.

ions in the ceria lattice, MCux series, probably due to the extrinsic defects created by the above-mentioned substitution. Activation energy for pure CeO_2, $FCeO_2$ (Fig. 7) and $MCeO_2$ (Fig. 8), obtained from measurements in the domain temperature of 573–1023 K, is about 0.45 and 0.51 eV, respectively, while it is found to be 0.43 eV and 0.25 eV in the case of 15 at.% Cu-substituted samples (FCu15 and MCu15, respectively). No noticeable variation in activation energy is observed for materials prepared by freeze-drying FCux with the copper content. In contrast, Arrhenius plots (Fig. 8) for cerium oxide reference material ($MCeO_2$) and Ce–Cu samples (MCux), prepared by microemulsion method, undergo significant changes according to dopant level. This phenomenon is in agreement with the physicochemical characterisation results presented in this study.

4. Conclusions

In this work, the synthesis of Ce–Cu mixed oxides with fluorite structure has been pursued. These materials do not display significant segregation of copper to the surface of the solid. All samples are nanosized materials with high surface area. Microemulsion coprecipitation method allows to obtain samples containing up to ca. 21 at.% Cu, mainly in substitutional positions in the mentioned fluorite network. Unfortunately, there is no evidence of copper incorporation to the ceria lattice for freeze-drying synthesised materials, FCux series. A thorough characterisation is necessary to elucidate the structure of these materials.

Although, it is still early for the proposal of these materials as SOFC anodes, physicochemical characterisation, specially thermal expansion coefficients and electrical conductivity measurements, suggests that substitutionally Ce–Cu binary mixed oxides having fluorite structure and high quantities of copper (>20 at.%) may be proposed as alternative SOFC anodes. Further research is required to optimise these materials, particularly to maximise electrical conductivity under reducing conditions. This study should be considered as an approach to get alternative anodes for solid oxide fuel cells that directly utilise hydrocarbon fuels.

Acknowledgements

This study is supported by the Community of Madrid (Program ENERCAM-CM, Ref. S-505/ENE-304) and Spanish Ministry of Education and Science (Project MAT2005-02933).

References

[1] A. Atkinson, S. Barnett, R.J. Gorte, J.T.S. Irvine, A.J. McEvoy, M. Mongensen, S.C. Singhal, J. Vohs, Nature 3 (2004) 17–27.
[2] S. McIntosh, J. Vohs, R.J. Gorte, Electrochim. Acta 47 (2002) 3815–3821.
[3] O. Costa-Nunes, R.J. Gorte, J.M. Vohs, J. Power Sources 141 (2005) 241–249.
[4] S. McIntosh, R.J. Gorte, Chem. Rev. 104 (2004) 4845–4865.
[5] H. Kim, J.M. Vosh, R.J. Gorte, J. Chem. Soc. Chem. Commun. (2001) 2334–2335.
[6] D. Vie, E. Martinez, F. Sapina, J.V. Folgado, A. Beltran, R.X. Valenzuela, V. Cortes-Corberan, Chem. Mater. 16 (2004) 1697–1703.
[7] V. Uskokovic, M. Drofenik, Surf. Rev. Lett. 12 (2005) 239–277.

[8] X.-C. Zheng, S.-H. Wu, S.-P. Wang, S.-R. Wang, S.-M. Zhang, W.-P. Huang, Appl. Catal. A 283 (2005) 217–223.
[9] W. Shan, W. Shen, C. Li, Chem. Mater. 15 (2003) 4761–4767.
[10] S.C. Singhal, K. Kendal, High Temperature Solid Oxide Fuel Cells: Fundamentals, Design and Application, Elsevier, 2003.
[11] A. Tomita, S. Teranishi, M. Nagao, T. Hibino, M. Sano, J. Electrochem. Soc. 153 (2006) A956–A960.
[12] A. Gayen, K.R. Priolkar, A.K. Shulka, N. Ravishankar, M.S. Hedge, Mater. Res. Bull. 40 (2005) 421–431.